

A New Probe of Cosmic Strings at LIGO and Mid-band: Gravitational Lensing Fringe

Sunghoon Jung^{1,*} and TaeHun Kim^{1,†}

¹*Center for Theoretical Physics, Department of Physics and Astronomy,
Seoul National University, Seoul 08826, Korea*

Cosmic strings are important remnants of early-Universe phase transitions. We show that they may be probed in a new way with LIGO and future gravitational-wave (GW) detectors. When the GW from compact binary mergers passes by a cosmic string, it is gravitationally lensed and left with a characteristic and detectable signal – the GW fringe. High-frequency detectors such as aLIGO and Einstein Telescope (ET) are favored in order to observe many numbers of fringe periods. But if they are augmented by mid-frequency detectors such as Atom Interferometer (AI) and Big Bang Observatory (BBO), the broadband ($f \simeq 0.1 - 1000$ Hz) detections can have significantly better fringe resolutions, hence enhanced sensitivities to the unconstrained parameter space ($G\mu \lesssim 10^{-7}$) of cosmic strings.

CONTENTS

I. Introduction	1
II. Lensing fringe from cosmic strings	2
A. Straight strings	2
B. Loops	4
III. Lensing Detection Calculation	5
A. Lensing detection criteria	6
B. Detection rate calculation	6
IV. Prospects	8
V. Discussion	11
A. Distinction from point-mass lens	11
B. Comparison with femto-lensing	11
C. Robustness against astrophysical uncertainties	11
VI. Conclusion	12
Acknowledgments	12
References	12

I. INTRODUCTION

It is believed that the early Universe has evolved down to the Standard Model from a more unified or fundamental theory by experiencing several phase transitions. The spontaneous symmetry breaking of a (global or gauge) $U(1)$ symmetry must have produced cosmic strings [1]. Cosmic strings are one-dimensional topological field configurations, produced also from string theory and vortex-like solutions of quantum field theory. Once produced, cosmic strings gradually evolve into the scaling regime, where the total energy density of strings and closed string loops remains constant with the expansion of the Universe [2–5]. Thus, observing cosmic strings that remain today can give important clues on the physics of the early Universe.

* sunghoonj@snu.ac.kr

† gimthcha@snu.ac.kr

Cosmic strings are characterized by its tension μ (energy density per unit length), given by $G\mu = v^2/m_{\text{P}_1}^2$ with the symmetry-breaking vacuum expectation value, v , of a $U(1)$ symmetry. The thickness of gauge strings is small of order $1/v$ so that it is a highly localized one-dimensional energy clump. The global string has its energy more spread in space stored in the Goldstone fields wrapping around the string. But their gravitational effects on null rays (photons and GWs as in this paper) are almost equivalent up to a marginal logarithm factor that describes the spatial spread [6]. String's high local energy density disturbs the homogeneity of the CMB power spectrum, hence constrained to be $G\mu \lesssim 10^{-7}$ (or $\Delta \lesssim 10^{-6}$ as will be introduced) [7]. Although cosmic strings consequently cannot be the dominant fraction of dark matter (DM) or the seed of structure formation, their high local energy density may still leave important observable signatures.

Cosmic strings have been probed mainly by CMB anisotropies, the stochastic GW radiated from gauge string loops, and by their gravitational lensing on photons. The GW radiation from string loops is an essential energy-loss mechanism in the evolution of a string network into the scaling regime, where the string network's energy density can remain safely small [2–5]. Thus, the stochastic GW is a prime observable that is actively searched for [8–10] (this may lead to a constraint as strong as $G\mu \lesssim 10^{-11}$, albeit model dependencies and debates), and its spectrum can also probe the cosmological evolution history of the Universe [11, 12]. But global string loops decay away rapidly by radiating off Goldstone bosons, thus the stochastic GW signal is absent. Instead, the order one number of long (at least Hubble-sized) strings per horizon always remain [13–15], as the causality requires. The long string can produce, e.g., gravitationally lensed images of a bright source behind it [16, 17]. These searches will extend the limit on $G\mu$, but more independent ideas are needed to probe a larger range of the parameter space of cosmic strings.

In this paper, we show that cosmic strings may be probed in a new way by aLIGO and future GW detectors. The new observable is based on the gravitational lensing of the GW from compact binary mergers by cosmic strings. Although the lensing effects on the photon have been studied [18, 19], the effects on the GW differ in several aspects in phenomenology and detection prospects, as will be discussed. Remarkably, with the new observable, aLIGO alone may have a sensitivity to the unconstrained parameter space of cosmic strings, in a way similar to the aLIGO's sensitivity to compact DM [20, 21]. But we also find that the cosmic string can be much better probed in extended broadband measurements, which can be realized by a combination of LIGO-band detectors with lower-frequency detectors; see also Refs. [22–26] for other examples of broadband benefits.

We start by discussing the lensing physics of cosmic strings and introducing the new observable in Sec. II, and we discuss lensing detection calculation in Sec. III, show and analyze detection prospects in Sec. IV, discuss further phenomenology in Sec. V, and conclude at the end.

II. LENSING FRINGE FROM COSMIC STRINGS

A. Straight strings

The space-time geometry around a (gauge) straight cosmic string is described by a conical space [16]

$$ds^2 = dt^2 - dZ^2 - dR^2 - \left(1 - \frac{\Delta}{2\pi}\right)^2 R^2 d\hat{\phi}^2, \quad (1)$$

where the string is placed along the Z axis and $\hat{\phi}$ is measured around the string. By the redefinition of the azimuthal angle $\phi = (1 - \Delta/2\pi)\hat{\phi}$, the conical space can be viewed as the Euclidean flat space with a deficit angle $\Delta \equiv 8\pi G\mu$. The deficit angle is defined by a boundary condition $h(\phi = 0) = h(\phi = 2\pi - \Delta)$ on the plane perpendicular to the string, with the allowed range $0 \leq \phi \leq 2\pi - \Delta$. The gravitational effect of global strings on null rays is described by a similar deficit angle [6]; thus, we simply use the same metric and lensing calculation for both cases.

There is a freedom to choose the direction of $\phi = 0$ in mapping the conical space to the Euclidean space with deficit angle. In the presence of a GW source, it is particularly convenient to choose that $\phi = 0$ is mapped to point to the source in the conical space. In the Euclidean space, this is equivalent to the source located at $\phi = 0$ and $\phi = 2\pi - \Delta$ simultaneously. Then the boundary condition of the deficit angle is automatically satisfied. Now, within the allowed range of ϕ , null rays from the source are propagated according to the usual Helmholtz equation on the Euclidean space. Consequently, the GW rays arriving at the observer can be obtained by the Kirchhoff diffraction integral of freely propagating rays around the string [27].

The gravitationally lensed GW waveform (that an observer measures) is parameterized in the frequency domain as

$$\tilde{h}^L(f) = \tilde{h}(f) F(f) e^{if\phi_m}. \quad (2)$$

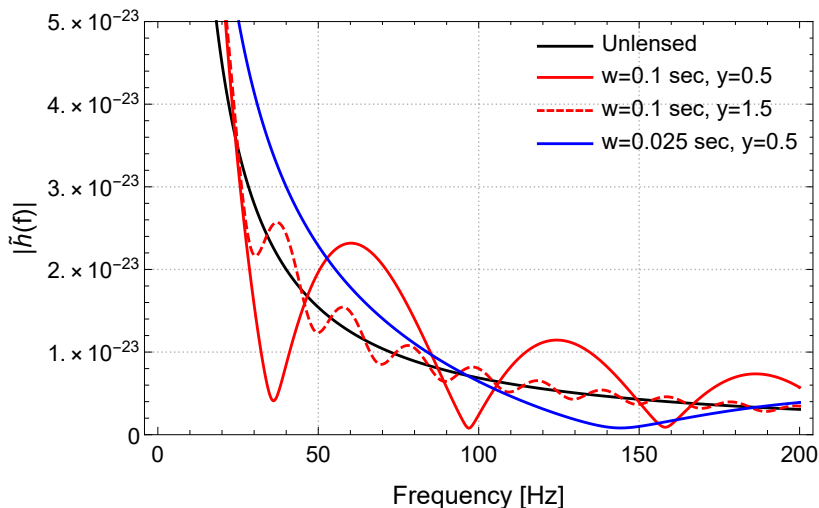


FIG. 1. GW fringe in the frequency domain. GW waveforms from $30M_{\odot}$ - $30M_{\odot}$ binary at 400 Mpc of luminosity distance: unlensed (black), lensed by a cosmic string with $w = 0.1$ sec and $y = 0.5$ (red-solid), $w = 0.1$ sec and $y = 1.5$ (red-dashed), $w = 0.025$ sec and $y = 0.5$ (blue). The characteristic path difference w and angular parameter y are defined in Eq. (4) and below.

Here, $\tilde{h}(f)$ is the unlensed waveform which is explained in Sec. III A. The complex lensing amplification $F(f)$ is the solution of the diffraction integral [18]

$$F(f) = e^{-i\frac{fw}{2}(1+2y)} \left\{ 1 - \frac{1}{2} \operatorname{erfc} \left[\sqrt{\frac{fw}{2i}}(1+y) \right] \right\} + e^{-i\frac{fw}{2}(1-2y)} \left\{ 1 - \frac{1}{2} \operatorname{erfc} \left[\sqrt{\frac{fw}{2i}}(1-y) \right] \right\}, \quad (3)$$

where

$$w \equiv 2\pi \frac{d_L d_{LS}}{d_S} \left(\frac{\Delta}{2} \right)^2 \approx 1.61679 \text{ sec} \times \left(\frac{d_L}{100 \text{ Mpc}} \right) \left(\frac{d_{LS}}{100 \text{ Mpc}} \right) \left(\frac{100 \text{ Mpc}}{d_S} \right) \left(\frac{\Delta}{10^{-8}} \right)^2 \quad (4)$$

is the characteristic path difference among the GW rays. $y \equiv 2\phi_S/\Delta$, where ϕ_S is the azimuthal angle ϕ between the two lines, the one connecting the observer and the string and the other connecting the string and the source, on the plane perpendicular to the string. As physics is symmetric with respect to $y \rightarrow -y$, hereafter we deal with only $y > 0$. We denote the luminosity distance by D , comoving distance by χ , and angular diameter distance by d ; the subscript L, S and LS denotes the distance to the lens, source and between the lens and source, respectively. As the lensing amplification $F(f)$ depends on w , in which the distances and Δ are packed into one variable, distances and Δ cannot be measured separately from the observed waveform alone. Lastly, the extra phase in Eq. (2)

$$\phi_m = \frac{w}{2} + wy \quad (5)$$

makes the arrival time of the fastest path to zero so that we can focus only on the relative phases among the rays; this shall be consistent with our choice of $t_c = 0$ in the GW waveform as discussed in Sec. III A.

In Fig. 1, we show an example unlensed waveform $|\tilde{h}(f)|$ and its lensed waveforms $|\tilde{h}^L(f)|$ in various lensing environments. The lensed waveforms oscillate with respect to the unlensed waveform, having local maxima at regular intervals. The oscillation is due to the interference between the rays contributing to the $F(f)$. We name this *interference fringe* in the frequency domain as the ‘‘GW fringe’’ [20, 28]; as will be discussed, the GW fringe from cosmic strings has several features different from the fringe generated by compact DM [20]. The oscillation is a key property of the GW fringe that allows efficient detection of lensing and distinction from other perturbations.

The GW fringe from the cosmic string is characterized by its maximum amplification and its width in the frequency domain. For $y < 1$, the interference occurs maximally so that $|F|$ oscillates from near 0 to near 2 in the whole range of f , for any values of w and y . This maximal interference can be seen in the red and blue lines (with $y = 0.5$) in Fig. 1. For $y = 1$, the amplitude of the interference is decreased by half, and still independent of w . On the other hand, for $y > 1$, the amplitude of the interference is smaller and decreases for an increase of f , w , and y . The red dashed line ($y = 1.5$) in the figure shows the smaller fringe amplitude which also decreases with increasing f . Lastly, all three cases show that the fringe width is smaller for greater w and y but constant over f . The dependence of the

fringe width on w is observed by comparing the red and the blue lines in the figure (the blue line has only the first minimum point near $f = 150$ Hz), and the dependence on y is observed from the red and the red dashed lines.

The GW fringe can be better understood in the limit $fw \gg 1$ (or, more precisely, $fw(1 \pm y)^2 \gg 1$), in which the phase shifts among the rays ($\sim fw$) span many numbers of the fringe period. In this limit, the amplification factor becomes the interference among *three* rays

$$F(f) \approx e^{-i\frac{fw}{2}(1+2y)} + \frac{1 + \text{sgn}(1-y)}{2} e^{-i\frac{fw}{2}(1-2y)} - \frac{2}{\sqrt{2\pi fw}(1-y^2)} e^{i(\frac{fw}{2}y^2 + \frac{\pi}{4})}. \quad (6)$$

We identify the first two terms as the result in the geometrical optics limit and the last term as a diffracted ray. For $y < 1$, the geometrical part has two terms for the two deflected rays in each side of the string; equivalently, in the Euclidean space with a deficit angle, the two rays arrive at us straightly from the two images of the source at $\phi = 0$ and $\phi = 2\pi - \Delta$. These two correspond to the usual two rays in the geometrical optics limit of the point-mass lensing. But important differences are: one of them (the second term in Eq. (6)) gets its amplitude decreased by half for $y = 1$ and disappears for $y > 1$, and finally that the third ray from diffraction also interferes in the cosmic-string case. Readers may refer to Fig. 3 in Ref. [29] for the ray diagram projected onto the plane perpendicular to the string, with cautions for slightly different notations.

The third term in Eq. (6) is the ray diffracted from the cosmic string. The diffracted nature is encoded in both the amplitude and the phase. The phase (or path difference) implies that this ray first hits the string and then goes to the observer, rather than going directly to the observer like the other two geometric rays. The decreasing amplitude with increasing f is also a common phenomenon of diffraction. We note that this third term is exactly derived by the geometric theory of diffraction [30]. Lastly but importantly, the diffracted ray weakens with increasing y , but this ray is one of the major contributions to the GW fringe for $y > 1$ since only one geometric ray can reach the observer in this regime.

In all, we can describe the GW fringe as follow. For $y < 1$, all three rays reach the observer, and the two geometric rays make a full interference while the effect of the diffracted ray is relatively suppressed. For $y = 1$, the amplitude of one geometric ray decreases to half, so a half-maximum interference occurs while the diffracted ray is still relatively suppressed. However, for $y > 1$, only one geometric ray can reach the observer, so the GW fringes are the result of interference between this ray and the diffracted ray. Hence the amplitude of the fringes is proportional to the amplitude of the diffracted ray, proportional to $1/\sqrt{fw}(1-y^2)$.

From Eq. (6), we can also estimate the fringe width f_{width} in the frequency domain. It is determined by the path difference among the major interfering rays – two geometric rays for $y \leq 1$ and one geometric ray and the diffracted ray for $y > 1$ – so that f_{width} times the path difference equals to the unity. By reading the path differences from the phase terms in Eq. (6), we obtain

$$f_{\text{width}} \simeq \begin{cases} \pi/wy, & \text{for } y \leq 1 \\ 4\pi/w(1+y)^2, & \text{for } y > 1 \end{cases}. \quad (7)$$

For example, the width $f_{\text{width}} \approx 0.04$ Hz for $\Delta = 10^{-7}$, $d_L = d_{LS} = 100$ Mpc, $d_S = 200$ Mpc, and $y = 1$ (giving $w \approx 81$ sec). In any case, the width is constant for the given string and source, so fringes repeat with a constant period as discussed and shown in Fig. 1.

B. Loops

The gauge string accompanies loops. The loops can survive for a long time as they decay slowly only by radiating off GWs; on the other hand, global string loops decay away within a few oscillations by radiating off Goldstone bosons [14]. Thus, the major fraction of the energy of a gauge string network may reside in the loop. In the scaling regime, the energy fraction of straight strings and loops remains a constant. In this subsection, to estimate loop's gravitational effect on the GW, we first calculate the total length of the loops and then the fraction of loops that can be treated as a straight string in the lensing perspective.

We assume the one-scale model [31] with the matter-dominated universe. In the one-scale model, all the loops formed at time t_B has its length at birth as $L(t_B) = \alpha l(t_B)$, where $l(t)$ is the particle horizon at time t and α is the free parameter of the model. Until we choose a specific value of α at the end of this section for further numerical calculation, we consider a fairly wide range of $\alpha = 0.1 \sim 10^{-5}$ [31]. Once a loop is formed, it radiates GW and shrinks with the energy-loss rate $dE/dt = -\Gamma G\mu^2$ with $\Gamma \approx 50$ being the constant determined by numerical simulation [31]. Then the length weighted comoving number density distribution at some given time becomes [32]

$$L \frac{dn(t)}{dL} \approx C' H_0^2 \frac{L}{(L + \frac{1}{3}\Gamma G\mu l(t))^2}, \quad (8)$$

where $n(t)$ is the total comoving number density of the loops at time t , H_0 is the Hubble parameter now, and C' is a constant to be determined by numerical simulations. In deriving this equation, $l(t) = 3t$ for the matter dominated universe and $\alpha \gg \Gamma G\mu$ are used. Until now, the time dependency is kept. However, in calculating the density fraction parameter Ω_{loop} , the time dependency finally drops out as expected from the scaling regime. The density fraction becomes

$$\Omega_{\text{loop}} \approx \frac{8\pi}{3} G\mu C' \left[\ln \left(\frac{3\alpha}{\Gamma G\mu} \right) - 1 \right], \quad (9)$$

which is time independent. Meanwhile, the number of infinite string in a Hubble volume can also be calculated via simulations [13, 31] and while there are some uncertainties they all give one or few infinite strings in a Hubble volume; similarly, the number of global strings is thought to be the order one per Hubble volume [14, 15]. In this work, we simply take the string number density to be one in a Hubble volume, so that $\Omega_\infty = 8\pi G\mu/3$. Therefore, the ratio of total loops to total straight strings is

$$\frac{\Omega_{\text{loop}}}{\Omega_\infty} = C' \left[\ln \left(\frac{3\alpha}{\Gamma G\mu} \right) - 1 \right]. \quad (10)$$

This is rather a generic result of the one-scale model. We use $\Gamma = 50$ and $C' = 0.625$, where the latter choice is the one we found to fit the recent simulation result [33]. The ratio can be calculated as a function of Δ and α . For the range of these parameters under our consideration, the minimum value $\Omega_{\text{loop}}/\Omega_\infty \approx 1.1$ is obtained with $\Delta = 10^{-6}$ and $\alpha = 10^{-5}$, and it grows as Δ decreases and α increases to become 12.6 for $\Delta = 10^{-10}$ and $\alpha = 0.1$. Thus, while the ratio $\Omega_{\text{loop}}/\Omega_\infty$ depends on the string tension $G\mu$ and the free parameter α , a large fraction of string network's energy reside in the loops for the most part of parameter space that we consider.

But will the loops give different lensing features from straight strings? While a loop is the same as a straight string in the vicinity of the loop segment, the far field metric (for distances much longer than the loop size) is the Schwarzschild metric with the total mass of the loop. Whether a loop segment gives the same lensing effect as a straight string is decided by whether it produces a pair of double images of a source behind it. By assuming all the loops to be oriented to face the observer, a loop at angular diameter distance d can always be regarded as a straight string if the loop radius r is bigger than $d\Delta/2$ [34]. In terms of the loop length L and comoving distance χ , this means

$$L > 8\pi^2 G\mu a(t(\chi)) \chi, \quad (11)$$

where $a(t)$ is the scale factor at time t and $t(\chi)$ is the traced-back time for a comoving distance χ ; if a photon is emitted at comoving distance χ and observed now, $t(\chi)$ is the age of the universe at the emission of the photon.

For a given χ , the total fraction of the loop length that can be treated as a straight string is approximately given by the length distribution Eq. (8) integrated over the range that satisfies Eq. (11) as

$$\xi_l(\alpha, \Delta, \chi) \approx \frac{\int_{8\pi^2 G\mu a(t)\chi}^{\alpha l(t)} L/[L + \frac{1}{3}\Gamma G\mu l(t)]^2 dL}{\int_0^{\alpha l(t)} L/[L + \frac{1}{3}\Gamma G\mu l(t)]^2 dL}. \quad (12)$$

Here, the upper bound comes from the longest loops at time $t(\chi)$. For a typical distance of 10^3 Mpc, the fraction is $\xi_l \approx 0.97$ for the smallest $\alpha = 10^{-5}$ and the largest $\Delta = 10^{-6}$ that we consider. It further increases and approaches to the unity for any other values of α and Δ , so here we conclude that most of the total loop-length can be treated as a straight string.

In all, in our final results, we assume that 100% of gauge string loops are treated as a straight string in our lensing study, and we use the energy fraction $\Omega_{\text{loop}}/\Omega_\infty$ calculated as above with $\alpha = 0.05$ [33].

III. LENSING DETECTION CALCULATION

We turn to discuss the detection criteria of the GW fringe and its detection-rate calculation. The most important feature of the GW fringe is that the lensed waveform oscillates with respect to the unlensed one (in the frequency domain) as shown and discussed in Fig. 1. Thus, being able to observe *many* and *large* enough oscillations is a key condition for the lensing detection. The lensing-detectability will be studied based on a simplified best-fit analysis. The detection rate will be calculated by integrating over all possible source and string locations for detectable lensing (but we do not separately calculate the lensing optical depth of a given source).

A. Lensing detection criteria

To ensure that *many* and *large* enough GW fringe oscillations are observed, we set three criteria that a detectable GW fringe should satisfy. First, the GW itself should be detected confidently. We require the signal-to-noise ratio (SNR) to be bigger than 10. This is slightly higher than the widely used value of 8, in order to safely see the lensing effect through the waveform of the detected GW signal. When we consider multiple detectors, we require the total SNR, each SNR summed in quadrature, to be larger than 10.

Secondly, the detected GW signal should be discriminated from the unlensed one. Following Ref. [20], we use the χ^2 least-squares fit to test this (here, we assume to claim that the lensing is detected if the lensed waveform cannot be fit well by unlensed ones)

$$\text{SNR}_{\text{test}} \equiv \left[4 \int_{f_{\min}}^{f_{\max}} \frac{|\tilde{h}^L(f) - \tilde{h}_{\text{best-fit}}(f)|^2}{S_n(f)} df \right]^{1/2} > 3, \quad (13)$$

where $S_n(f)$ is the power spectrum of the noise and $f_{\min, \max}$ are the frequency range of the considered measurement; we always integrate up to the innermost stable circular orbit $f_{\max} = f_{\text{ISCO}} = (6\sqrt{3}\pi M)^{-1}$. The $\tilde{h}_{\text{best-fit}}(f)$ is the unlensed GW waveform which minimizes the SNR_{test} . Finding this best-fit proceeds by optimizing selected parameters of the unlensed waveform. Following Ref. [20], we use the following unlensed waveform $\tilde{h}(f)$ for the lensing calculation in Eq. (2), and we simplify this for a two-parameter best-fit function $\tilde{h}_{\text{best-fit}}(f; A_0, \phi_0)$:

$$\tilde{h}(f) = \sqrt{\frac{5}{96}} \frac{\pi^{-2/3} \mathcal{M}_z^{5/6}}{D_S} f^{-7/6} e^{i\Psi(f)} \quad \rightarrow \quad \tilde{h}_{\text{best-fit}}(f; A_0, \phi_0) = A_0 f^{-7/6} e^{i\Psi(t_c=0) + i\phi_0}, \quad (14)$$

where D_S is the luminosity distance to the source, \mathcal{M}_z is the redshifted chirp mass, and the phase is $\Psi(f) = 2\pi f t_c + \frac{3}{128} (\pi \mathcal{M}_z f)^{-5/3}$ with t_c being the time of coalescence (or the integration constant from the Fourier transform). In the left-hand side, we have chosen particular (and optimal) values of the binary inclination and the GW projection along detector baselines, as an average over all possible directions of source and detectors, and we use the same values for all cases for simplicity. We ignore the time-variation of detector directions, for simplicity, either because measurement time is very short (so that they are almost constant) or their time variation (daily or hourly) is very different from the fringe oscillation. We use $t_c = 0$ for both $\tilde{h}^L(f)$ and $\tilde{h}(f)$. But, since the lensing does affect this time by shortening the fastest path from the source to the observer, we use ϕ_m in Eq. (2) to compensate this effect so that unobservable time difference becomes irrelevant to our study; only relative time shifts among the rays are important. Finally, in the right-hand-side, we fit the lensed waveform by the two fitting parameters: the overall amplitude A_0 and the overall phase-shift ϕ_0 . The constant A_0 is approximately good enough as we regard that \mathcal{M}_z can be measured precisely from the time evolution of the frequency and we ignore the time-dependence of detector directions. A similarly simplified approach used to study the point-mass lensing [20] turned out to be reasonable by comparing with more dedicated works later [35, 36].

Lastly, the frequency resolution should be good enough to see the interference fringes in the frequency domain. We demand that the fringe width should be larger than the twice the frequency resolution so that each fringe can be safely recognized. The fringe width is given by Eq. (7) with w in Eq. (4), and the minimum resolvable frequency is given by the inverse of the total measurement time T , which is given by

$$\begin{aligned} f_{\text{resolution}}(f_{\max}, f_{\min}, \mathcal{M}_z) &= \frac{8\pi}{5} (8\pi G \mathcal{M}_z)^{5/3} \left(\frac{1}{f_{\min}^{8/3}} - \frac{1}{f_{\max}^{8/3}} \right)^{-1} \\ &\approx 1.5457 \text{ Hz} \times \left(\frac{\mathcal{M}_z}{100 M_\odot} \right)^{5/3} \left(\frac{f_{\min}}{10 \text{ Hz}} \right)^{8/3}, \end{aligned} \quad (15)$$

where $f_{\min} \ll f_{\max}$ is used in the last approximation.

B. Detection rate calculation

The lensing detection rate is given by a product of the comoving merger-rate density, comoving cosmic-string density, and the 6-dimensional (6D) volume of a region in space of source position and cosmic string position which satisfies the three criteria in Sec. III A. We used all distances in comoving distance χ 's during the calculation, so all the volumes are comoving volumes. We assumed all the binary mergers are composed of two identical black holes

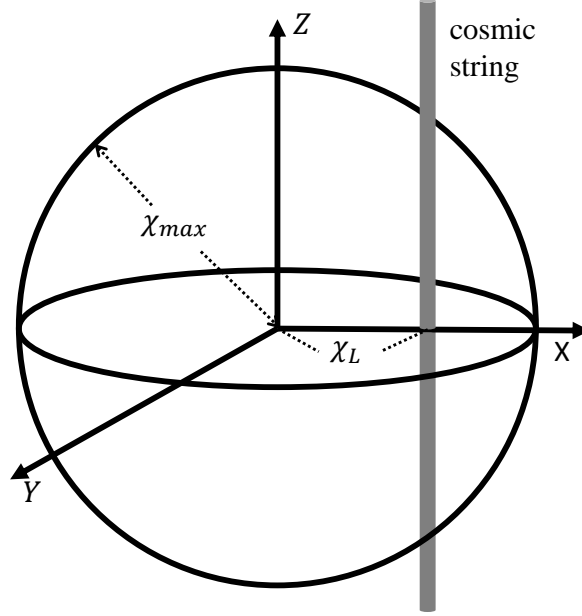


FIG. 2. Comoving coordinate system and the placement of a cosmic string used for the lensing detection calculation.

with mass M , so the chirp masses in Eq. (14) and (15) become $\mathcal{M} = 2^{-1/5}M$ (hereafter all the masses appearing are the redshifted ones). The comoving merger-rate density is calculated in [37] with the latest version in [38]; we take the M10 optimistic prediction at $z_S = 0.1$, denoted as $n_s(M)$. Here, $n_s(M)$ is given for several selected mass bins. The comoving cosmic string density is chosen to be one in a Hubble volume, $n_{cs} = [4.3 \times 10^3 \text{Mpc}]^{-3}$, by referring to the scaling solution [13–15, 31]. Both densities are assumed to be constant in redshift for simplicity, but $n_s(M)$ may increase with z_S [37].

The 6D volume, V_{6D} , depends on M , Δ , and the detection method $= \{f_{\max}, f_{\min}, S_n(f)\}$. The assumed homogeneity and isotropy of $n_s(M)$ and n_{cs} allow us to calculate the lensing detection (event) rate as

$$\text{Event rate}(\Delta, M; f_{\max}, f_{\min}, S_n(f)) = n_s(M) n_{cs} V_{6D}(\Delta, M; f_{\max}, f_{\min}, S_n(f)). \quad (16)$$

To calculate the V_{6D} , we first think of the 3D volume for source positions that give detectable lensing effect, when the string is placed at χ_L from the observer (see Fig. 2). This 3D volume is denoted by $V(\chi_L, \Delta, M; f_{\max}, f_{\min}, S_n(f))$. Then, V_{6D} is given by a volume integral of V with respect to the string position, so that

$$V_{6D}(\Delta, M; f_{\max}, f_{\min}, S_n(f)) = \int_0^\infty 4\pi\chi_L^2 V(\chi_L, \Delta, M; f_{\max}, f_{\min}, S_n(f)) d\chi_L. \quad (17)$$

Here we note that the string direction does not matter by the isotropicity, so picking an arbitrary direction is sufficient for our calculation.

To evaluate V for the given string distance χ_L , we first obtain the maximum comoving distance of the source, $\chi_{\max}(M; f_{\max}, f_{\min}, S_n(f))$, by requiring the unlensed SNR to be greater than 10. Using the unlensed SNR instead of lensed one is a convenient assumption for the calculation that will be detailed below, but it is also somewhat conservative in the sense that lensed SNR is often larger than the unlensed one. Then for any Δ , our interest of source position is limited to the sphere of radius χ_{\max} , which also makes $V(\chi_L > \chi_{\max}) = 0$. During the calculation, we use the Cartesian coordinate for the comoving grid (here we used the uppercase letters for the coordinates), placing the observer at the origin, cosmic string parallel to the Z -axis and the closest point to the observer on the X -axis (see Fig. 2).

Within the χ_{\max} , V is calculated by finding the maximum source distance on the Y -axis (for detectable lensing) for each point on the XZ plane, denoted as $Y_{\max}(X, Z)$. Then V is given by

$$V(\chi_L, \Delta, M; f_{\max}, f_{\min}, S_n(f)) = 2 \int_0^{\chi_{\max}} \int_{\chi_L}^{\chi_{\max}} Y_{\max}(X, Z) dXdZ, \quad (18)$$

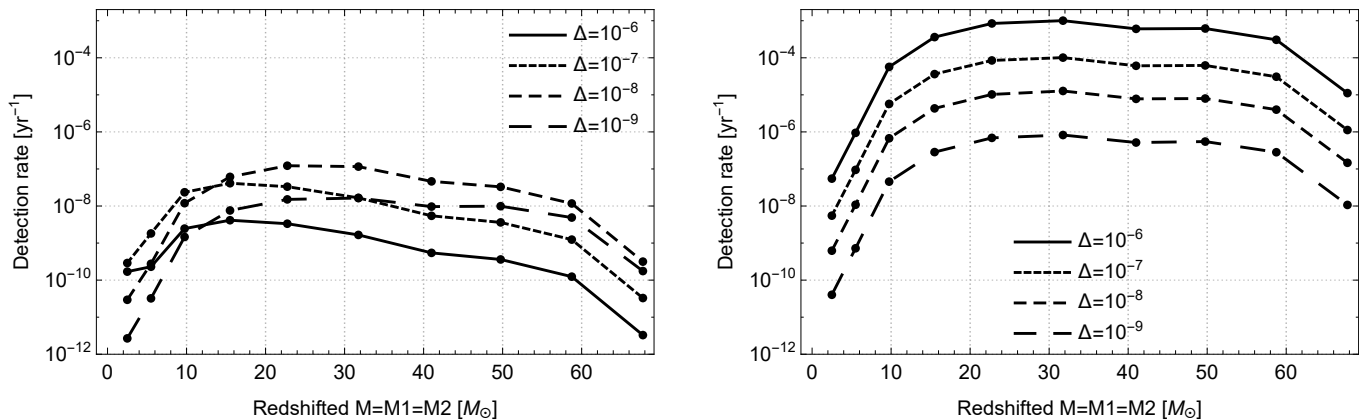


FIG. 3. Detection rate of the GW fringe with four aLIGOs alone (left) and with additional four AIs for the last one-week measurement (right), for a different deficit angle $\Delta = 8\pi G\mu$ for each curve.

where the factor two is from the $Y < 0$ region. Y_{\max} is determined by the two lensing-detection criteria on the SNR_{test} and the frequency resolution. Instead of calculating SNR_{test} in the 3-dimension (X, Y, Z) , equivalently we draw a contour plot of $\epsilon \equiv \text{SNR}_{\text{test}}/\text{SNR}$ in the w and y plane because the amplification F is a function of w and y . Both w and y depend on the point (X, Y, Z) as defined in Sec. II A. But the expansion of the universe redshifts the frequency so that $f_w = f_{\text{obs}}(1 + z_I)w$ in Eq. (2) and (3), where f_{obs} is the observed frequency and z_I is the redshift of the intersection point of the cosmic string and the line of sight from the observer to the source. So by using the observed f_{obs} in all calculations, all the w 's appearing in the equations are multiplied by a factor of $1 + z_I$. And $y = 2\phi_S/\Delta$ is expressed in this Cartesian coordinate as $y = 2 \tan^{-1} [Y/(X - \chi_L)]/\Delta$. Using the ϵ contour and the unlensed SNR on each point, we find the minimum required ϵ and finally y_{\max} . Then, we check whether this y_{\max} satisfies the frequency resolution criterion by Eq. (7) and (15). If it does, we convert y_{\max} to Y_{\max} using the aforementioned relation, but if it does not, we use Eq. (7) and (15) to get a new y_{\max} and corresponding Y_{\max} . In this way, we can find the Y_{\max} which satisfies the both criteria.

In the actual numerical evaluation of V (Eq. (18)) we divided each axis by 16 sectors and used rectangular quadrature, where the condition $\sqrt{X^2 + Z^2} \leq \chi_{\max}$ is inserted as a Boolean equation into the integrand (note that $Y_{\max} \ll X$ or Z). Similarly, the evaluation of V_{6D} (Eq. (17)) used the rectangular quadrature with 16 sectors for $0 \leq \chi_L \leq \chi_{\max}$.

IV. PROSPECTS

We turn to show detection prospects at aLIGO and future GW detectors. To be able to observe many enough fringe oscillations, high-frequency detectors are favored. As will be shown, the LIGO-band frequencies are high enough to detect GW fringes from $\Delta \lesssim 10^{-6}$ which is currently allowed. We start by discussing results from four aLIGO detectors with design sensitivity [39] and also from one ET detector [40], which probes the similar frequency band but with 10 – 50 times smaller noise than aLIGO. We will also find that the measurement time in this frequency band is too short to have good enough frequency resolutions. Thus, we will extend the frequency band by adding mid-frequency detectors – four AI detectors at the resonant mode [41, 42] or one BBO detector [43] – as a possible example to improve the resolution.

The detection prospects are shown in Fig. 3 – 6. Fig. 3 and 4 are about aLIGO and its extensions, and Fig. 5 and 6 are about ET and its extensions. In Fig. 3 and 5, we show detection rates as functions of M for several values of Δ . Then, in Fig. 4 and 6, we show the total detection rates per year as functions of Δ , by summing up the rates for all M bins.

In Fig. 3 and 5 left panels, we show detection rates of LIGO-band detectors alone. First of all, the detection rates typically decrease in both the small and large M limits. This is because too small M gives too small SNR (and hence smaller χ_{\max} with the correspondingly smaller detectable region), whereas too large M has too low merger-rate densities [37, 38]. Secondly, the overall detection rates grow with Δ (because lensing effects become stronger), but they are relatively suppressed for too large $\Delta \sim 10^{-7} - 10^{-6}$. This is because the fringe width becomes too small to be resolved within a short measurement time, particularly becoming a limiting factor for heavy binaries spending short time in the LIGO-band. It is more clearly shown in the Case 1 of Fig. 4 and 6. The maximum total detection

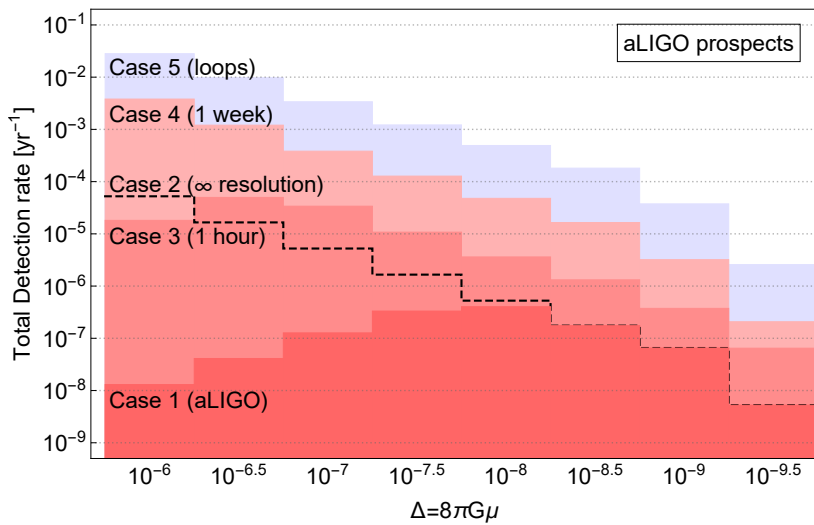


FIG. 4. Overlapped chart of total detection rate of the GW fringe with four aLIGOs. Case 1: four aLIGOs alone. Case 2 (dashed): Case 1 without frequency resolution restriction. Case 3: four aLIGOs plus four AIs, measurement done for the last one hour. Case 4: Case 3 with the last one week-measurement. Case 5: Case 4 with taking string loops into account.

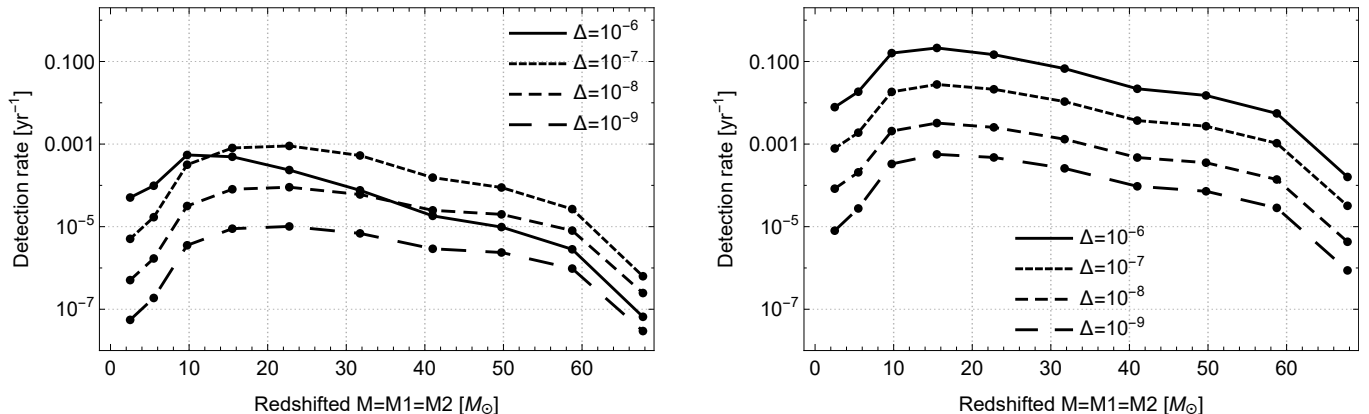


FIG. 5. Detection rate of the GW fringe with one ET alone (left) and with additional BBO for the last one-week measurement (right), for a different deficit angle $\Delta = 8\pi G\mu$ for each curve.

rates occur for $\Delta = \Delta_{\text{crit}} \sim 10^{-8}$ ($10^{-6.5}$) with aLIGO (ET) alone; these are where the fringe widths $f_{\text{width}} \sim \mathcal{O}(1 \text{ Hz})$ ($\mathcal{O}(10^{-3} \text{ Hz})$) in Eq. (7) and (4) become similar to the frequency resolutions in Eq. (15) with $f_{\text{min}} \sim 10$ (1) Hz.

To further confirm that the deficiency at large Δ is due to the frequency resolution, we attempt to try an infinite frequency resolution artificially. The results are drawn in dashed lines in Fig. 4 and 6 (Case 2). It shows that the total detection rates steadily increase for increasing Δ for both detectors, supporting our conclusion that the decrease of the total rate in the large- Δ region is due to the limited frequency resolution. In the range of $\Delta = 10^{-10}$ to 10^{-6} considered in this paper, the maximum total rate occurs at $\Delta = 10^{-6}$, giving $5.2 \times 10^{-5} \text{ yr}^{-1}$ for aLIGO and $3.2 \times 10^{-2} \text{ yr}^{-1}$ for ET. Both detectors receive significant improvements, and this implies that improving the frequency resolution will be an important aim in probing cosmic strings with large Δ values.

This leads us to consider combining mid-frequency detectors with LIGO-band detectors to allow a longer measurement time. Four AIs are added to four aLIGOs, and one BBO is added to one ET. The combination of detectors (which can measure a broadband including $f \simeq 0.1 - 1000 \text{ Hz}$ relevant to us) gives two strong improvements. First, a longer measurement time gives a better frequency resolution, so Δ_{crit} becomes larger. Second, it also gives higher SNR for a source at a given distance, so the overall lensing detectable volume increases (due to the enlargement of χ_{max} and Y_{max} given by the SNRtest). For these combined detectors, we assume fixed time measurements to see how the results improve with particular frequency resolutions. We consider one hour and one week of measurement times; the one-week measurement corresponds to $f \simeq 0.1 - 1000 \text{ Hz}$ for $30M_{\odot}$ - $30M_{\odot}$ binaries.

The results for the combined detectors are Case 3 and 4 (one hour and one week, respectively) in Fig. 4 and 6, and

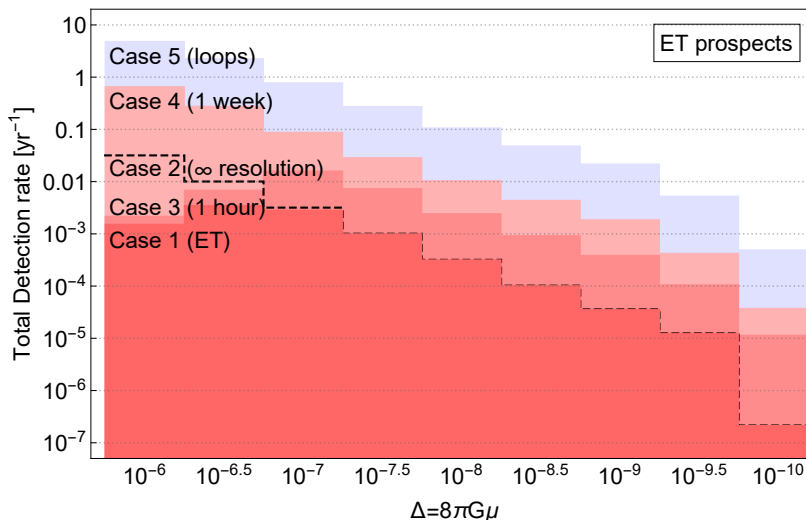


FIG. 6. Overlapped chart of total detection rate of the GW fringe with one ET. Case 1: one ET alone. Case 2 (dashed): Case 1 without frequency resolution restriction. Case 3: one ET plus one BBO, measurement done for the last one hour. Case 4: Case 3 with the last one-week measurement. Case 5: Case 4 with taking string loops into account.

the right panels of Fig. 3 and 5 (one week). Although the one-hour measurement raises Δ_{crit} for aLIGO results as expected, it does not raise Δ_{crit} for ET results. This is because that the sensitivity range (in the frequency domain) of aLIGO corresponds to a time interval that is much shorter than an hour, whereas that of ET, which reaches to a somewhat lower frequency than aLIGO, already corresponds to a time interval of the order of an hour. However, for both detectors in any case, the detection rates become a few times higher for the small- Δ region. It is due to the increase of the SNR. After all, one-hour measurements yield the maximum total detection rate at $\Delta_{\text{crit}} = 10^{-6.5}$ for aLIGO+AI giving $5.0 \times 10^{-5} \text{ yr}^{-1}$, and for ET+BBO at $\Delta_{\text{crit}} = 10^{-7}$ giving $1.6 \times 10^{-2} \text{ yr}^{-1}$. The values of Δ_{crit} can again be understood by comparing the frequency width with the frequency resolution: the minimum width from our criteria $f_{\text{width}} > 1/1800 \text{ Hz} \approx 5.6 \times 10^{-4} \text{ Hz}$ for one-hour (3600 sec) measurement becomes similar to the fringe width at $\Delta \sim 6 \times 10^{-7}$ (by assuming $y = 1$ and all the angular diameter distances of order 100 Mpc in Eq. (7) and (4)), which is close to the actual Δ_{crit} that we mentioned.

If we consider one-week measurements, as shown in Case 4 of Fig. 4 and 6 as well as right panels of Fig. 3 and 5, the frequency resolution is no longer a problem for both detectors. Thus the maximum occurs at $\Delta = 10^{-6}$ for both detectors, giving $3.8 \times 10^{-3} \text{ yr}^{-1}$ for aLIGO+AI and 0.66 yr^{-1} for ET+BBO.

Before moving on, we discuss the range of detectable Δ . For a set of detection method and M , the largest detectable Δ is limited by the frequency resolution since too high Δ makes the fringe width too small to be resolved, as discussed. On the other hand, the smallest detectable Δ is limited by too broad fringe width (or too small number of periods). For instance, at $y = 1$, we can estimate the number of fringes for frequency up to f , given by (from Eq. (7))

$$\text{Fringe number} = \frac{fw}{\pi} \sim \left(\frac{f}{200 \text{ Hz}} \right) \left(\frac{d}{100 \text{ Mpc}} \right) \left(\frac{\Delta}{10^{-9}} \right)^2, \quad (19)$$

where all the distance terms in w are assumed to be in the same order, denoted by d . For $M = 30M_{\odot}$, the fringe number up to $f_{\text{ISCO}} \approx 200 \text{ Hz}$ becomes about the unity for $d = 100 \text{ Mpc}$ and $\Delta = 10^{-9}$. This means that for about $\Delta \lesssim 10^{-10}$, there is effectively no fringe in the measurement range. To increase the number of fringes, d or y should increase, but the first option decreases SNR and the second option decreases the fringe amplitude. Therefore, both options may not increase SNRtest sizably. Thus, we understand that the smallest Δ that can be measured in this broadband detectors will be about $\Delta \sim 10^{-10}$, as shown in Fig. 4 and 6.

Now we add string loop contributions (for gauge strings) shown in Case 5 of Fig. 4 and 6. As discussed in Sec. II B, we use $\alpha = 0.05$ and take ξ_l to be the unity. Since $\Omega_{\text{loop}}/\Omega_{\infty}$ is the same for all four cases (Case 1 – 4), we present the results by adding loop contributions to the one-week measurements only. The results show that loops give order-one enhancement of the detection rates. Although $\Omega_{\text{loop}}/\Omega_{\infty}$ decreases for increasing Δ , the dependence is weak. The maximum detection rate is $2.8 \times 10^{-2} \text{ yr}^{-1}$ for aLIGO+AI and 4.8 yr^{-1} for ET+BBO, both at $\Delta = 10^{-6}$.

If the GW fringe is detected, a precision measurement can be performed to measure cosmic string parameters (see also Sec. V A for the distinction from point-mass lenses). On the other hand, null detection would impose an upper bound on Δ . However, our results are also subject to uncertainties from merger-rate and string densities. For

instance, the optimistic merger-rate density that we used (M10) is about 100-150 times larger than the M23 pessimistic merger-rate density [37, 38]. The cosmic string number density is also subject to the order-ten uncertainties among the simulations of string networks [13].

V. DISCUSSION

A. Distinction from point-mass lens

We further discuss that a cosmic string can be distinguished from a point-mass lens by looking at the interference pattern. For a cosmic string, both $y \leq 1$ and $y > 1$ cases each have differences from a point-mass case.

For $y > 1$, the amplitude of the interference fringe decreases as the GW frequency increases because the diffracted ray has its amplitude proportional to $1/\sqrt{f}$. But this is not the case for the point-mass lensing or the cosmic-string lensing with $y \leq 1$, because the interference for these cases is induced by two geometric rays. Therefore, if a detected GW signal has interference fringes that diminish with increasing f , this indicates that the lens is a cosmic string (with $y > 1$).

Cosmic strings with $y \leq 1$ can still be distinguished from a point-mass lens. In the frequency domain, the fringe-peak frequency for a point-mass lens [28, 44] is always $\pi/2$ shifted with respect to the cosmic string case [18] for the given fringe width. The shift is originated from a saddle-point contribution in the point-mass lensing, which does not exist in the cosmic string lensing. The shift can be measured by correlating the peak frequency with the fringe width. In the case of cosmic string (without the shift), $f_{\text{peak}} = n f_{\text{width}}$, while in the point-mass case (with the shift) the relation becomes $f_{\text{peak}} = (n + \frac{1}{4}) f_{\text{width}}$, where $n = (0, 1, 2, \dots)$. Thus, if the detected signal shows at least two peaks with good frequency resolution, such a correlation can be clearly identified.

B. Comparison with femto-lensing

The GW fringe is a GW counterpart of photon femtolensing [45]. Both observables are based on the lensing interference fringe, but they become observable by different reasons. The GW fringe is naturally observable through the chirping of GW (i.e. frequency changes in time); but the photon femtolensing is observable through the spectral fringe (so that stable and reliable source spectrum is needed). Often, gamma-ray bursts (GRBs) with $f \sim 10^{19}$ Hz or radio bursts are used in femtolensing observations. As the probe wavelengths of photons and GWs are so different, they can probe different ranges of the lens mass/energy. Both fringe observables are most readily observable when the probe wavelength is about the Schwarzschild radius of the lens so that the chirping or spectrum sweeps a $O(1 - 10)$ range of fringe periods. The condition can be written as (see Eq. (19))

$$fw \sim \left(\frac{f}{100 \text{ Hz}} \right) \left(\frac{D}{100 \text{ Mpc}} \right) \left(\frac{\Delta}{10^{-9}} \right)^2 \sim 1 \quad (20)$$

for the cosmic-string lensing and similarly as $f\Delta t_d \simeq 10^{14} \left(\frac{M_L}{M_\odot} \right) \sim 1$ for the point-mass lensing [20] with the typical time-delay $\Delta t_d = 4GM_L$ and the lens mass M_L . These translate into the different favored ranges of the lens mass for the fringe observation: the cosmic-string fringe from LIGO has $\Delta \sim 10^{-9}$ as discussed, and from GRB, $\Delta \sim 10^{-18}$ [18], and similarly for the point-mass fringe from LIGO has $M_L \sim 100M_\odot$ [20], and from GRB, $M_L \sim 10^{-14}M_\odot$ [46]. Obviously, the much longer wavelength of the GW can probe much heavier cosmic strings and compact DMs (still unconstrained by detection experiments).

C. Robustness against astrophysical uncertainties

The GW fringe can be subject to various uncertainties from string movements, source movements, and source size which all can blur the sharp fringe pattern. Indeed, these are one of the main uncertainties of photon femtolensing. But GW fringe is much more robust against them, mainly due to much longer wavelengths and relatively short measurement time. The fringe pattern can be erased if the source size or the source/string movements (during measurement time) $\delta\ell \simeq D\Delta\delta y$ becomes large enough so that the change $\delta y \gtrsim 1$ sweeps a whole fringe period. This limits the maximal source size or the source/string movements to be

$$\delta\ell \lesssim \left(\frac{D}{100 \text{ Mpc}} \right) \left(\frac{\Delta}{10^{-9}} \right) \cdot 3 \times 10^{15} \text{ km}. \quad (21)$$

The limit $\sim 10^{15}$ km for the GW fringe is likely to be well satisfied for any sources and strings during even week-long measurements (that we consider in this paper). But the limit becomes much stronger $\sim 10^6$ km for GRB femtolensing (with $\Delta \sim 10^{-18}$) [18, 47] and may critically limit the robust observation. In particular, cosmic strings can move relativistically so that the size limit $\sim 10^6$ km implies the measurement time to be less than about minutes or so.

The relativistic movement of strings can induce the GW frequency red/blue-shift, but it is negligibly small of the order $\delta f/f \simeq \Delta$ [48]. It also enhances the lensing deflection angle by the boost $\gamma = 1/\sqrt{1-v^2} \sim 1.3$ [49] (in average over the momentum direction) for a typical velocity $v \sim 2/3$ of relativistic strings. This effectively shifts the relevant Δ value by the γ factor. Although we ignore this effect, one can approximately account for this by using the shifted Δ in our results. In any case, a fringe pattern may change slightly but it will not be erased.

Moreover, the GW waveform from a binary inspiral is well predicted by general relativity, governed most importantly by the binary masses. This allows to detect tiny GWs and to test general relativity [50] as well as weak (DM-induced) fifth forces [26]. But astrophysical properties of GRB or radio bursts are under relatively poor control both theoretically and experimentally. Thus, the (cosmic-string) GW fringe is potentially a powerful precision observable of massive structures in the Universe.

VI. CONCLUSION

In this paper, we have studied a new way to probe the cosmic string at LIGO and future GW detectors. Unlike the well-known probe with the GW emitted from loops, our new observable – the GW fringe – detects the gravitational lensing on the binary GW passing by straight strings or large loops. The LIGO-band frequency turns out to be ideal to probe the unconstrained region $\Delta = 8\pi G\mu \lesssim 10^{-6}$, but the extension with lower-frequency detectors improve the sensitivity significantly.

The GW fringe is observable naturally through the chirping (the time-evolution of the frequency) of the binary GW. Thus the highest-frequency near-merger observations of LIGO-band detectors (aLIGO and ET in this paper) are essential. Combined with mid-frequency detectors (AI and BBO in this paper) to overcome the frequency-resolution limitation, the week-long measurement of each GW with $4 \times$ aLIGO+AI (ET+BBO) can potentially detect as many as 10^{-2} (10^0) GW fringes per year for $\Delta = 10^{-6}$, and 10^{-5} (10^{-2}) GW fringes for $\Delta = 10^{-9}$. Multi-year GW detections in this broadband ($f \simeq 0.1 - 1000$ Hz) will be able to probe the unconstrained parameter space of the cosmic string, $\Delta = 10^{-6} \sim 10^{-10}$, in this new way.

Our study also emphasizes that the long-time highest-frequency measurements in the broadband $f \simeq 0.1 - 1000$ Hz can potentially provide good precision capabilities [22–26] to probe massive structures in the Universe. In addition, being relatively robust against astrophysical uncertainties, the GW fringe is potentially a good precision observable. These shall motivate the development of mid-frequency GW detectors (such as AI and BBO in this paper that are targeted for relatively farther future) which can combine with upcoming LIGO-band detectors to measure such a broadband. The early Universe with cosmic strings is one example physic case, and some DM candidates [20, 21] and even larger-scale structures may also be probed in this broadband with the GW fringe.

ACKNOWLEDGMENTS

We thank Yanou Cui, David E. Morrissey, Yi Wang and Chul-Moon Yoo for useful comments. Our work is supported by National Research Foundation of Korea under grant 2015R1A4A1042542, 2017R1D1A1B03030820, by Research Settlement Fund for the new faculty of Seoul National University, and by POSCO Science Fellowship.

-
- [1] T. W. B. Kibble, “Some Implications of a Cosmological Phase Transition,” *Phys. Rept.* **67**, 183 (1980). doi:10.1016/0370-1573(80)90091-5
 - [2] V. Vanchurin, K. D. Olum and A. Vilenkin, “Scaling of cosmic string loops,” *Phys. Rev. D* **74**, 063527 (2006) doi:10.1103/PhysRevD.74.063527 [gr-qc/0511159].
 - [3] J. V. Rocha, “Scaling solution for small cosmic string loops,” *Phys. Rev. Lett.* **100**, 071601 (2008) doi:10.1103/PhysRevLett.100.071601 [arXiv:0709.3284 [gr-qc]].
 - [4] T. W. B. Kibble, “Topology of cosmic domains and strings,” *J. Phys. A* **9**, 8 (1976) doi:10.1088/0305-4470/9/8/029.
 - [5] A. Vilenkin, “Cosmic Strings and Domain Walls,” *Phys. Rept.* **121**, 263 (1985). doi:10.1016/0370-1573(85)90033-X
 - [6] D. Harari and P. Sikivie, “The Gravitational Field of a Global String,” *Phys. Rev. D* **37**, 3438 (1988). doi:10.1103/PhysRevD.37.3438

- [7] T. Charnock, A. Avgoustidis, E. J. Copeland and A. Moss, “CMB constraints on cosmic strings and superstrings,” *Phys. Rev. D* **93**, no. 12, 123503 (2016) doi:10.1103/PhysRevD.93.123503 [arXiv:1603.01275 [astro-ph.CO]].
- [8] S. Kuroyanagi, K. Miyamoto, T. Sekiguchi, K. Takahashi and J. Silk, “Forecast constraints on cosmic strings from future CMB, pulsar timing and gravitational wave direct detection experiments,” *Phys. Rev. D* **87**, no. 2, 023522 (2013) Erratum: [*Phys. Rev. D* **87**, no. 6, 069903 (2013)] doi:10.1103/PhysRevD.87.069903, 10.1103/PhysRevD.87.023522 [arXiv:1210.2829 [astro-ph.CO]].
- [9] J. J. Blanco-Pillado, K. D. Olum and X. Siemens, “New limits on cosmic strings from gravitational wave observation,” *Phys. Lett. B* **778**, 392 (2018) doi:10.1016/j.physletb.2018.01.050 [arXiv:1709.02434 [astro-ph.CO]].
- [10] C. Ringeval and T. Suyama, “Stochastic gravitational waves from cosmic string loops in scaling,” *JCAP* **1712**, no. 12, 027 (2017) doi:10.1088/1475-7516/2017/12/027 [arXiv:1709.03845 [astro-ph.CO]].
- [11] Y. Cui, M. Lewicki, D. E. Morrissey and J. D. Wells, “Cosmic Archaeology with Gravitational Waves from Cosmic Strings,” *Phys. Rev. D* **97**, no. 12, 123505 (2018) doi:10.1103/PhysRevD.97.123505 [arXiv:1711.03104 [hep-ph]].
- [12] Y. Cui, M. Lewicki, D. E. Morrissey and J. D. Wells, “Probing the pre-BBN universe with gravitational waves from cosmic strings,” arXiv:1808.08968 [hep-ph].
- [13] R. Consiglio, O. Sazhina, G. Longo, M. Sazhin and F. Pezzella, “On the number of cosmic strings,” *Mon. Not. Roy. Astron. Soc.* **439**, no. 4, 3213 (2014) doi:10.1093/mnras/stu048 [arXiv:1112.5186 [astro-ph.CO]].
- [14] D. Harari and P. Sikivie, “On the Evolution of Global Strings in the Early Universe,” *Phys. Lett. B* **195**, 361 (1987). doi:10.1016/0370-2693(87)90032-3
- [15] P. Sikivie, “Cosmic global strings,” *Phys. Scripta T* **36**, 127 (1991). doi:10.1088/0031-8949/1991/T36/014
- [16] A. Vilenkin, “Gravitational Field of Vacuum Domain Walls and Strings,” *Phys. Rev. D* **23**, 852 (1981). doi:10.1103/PhysRevD.23.852
- [17] J. R. Gott, III, “Gravitational lensing effects of vacuum strings: Exact solutions,” *Astrophys. J.* **288**, 422 (1985). doi:10.1086/162808
- [18] C. M. Yoo, R. Saito, Y. Sendouda, K. Takahashi and D. Yamauchi, “Femto-lensing due to a Cosmic String,” *PTEP* **2013**, 013E01 (2013) doi:10.1093/ptep/pts045 [arXiv:1209.0903 [astro-ph.CO]].
- [19] T. Suyama, T. Tanaka and R. Takahashi, “Exact wave propagation in a spacetime with a cosmic string,” *Phys. Rev. D* **73**, 024026 (2006) doi:10.1103/PhysRevD.73.024026 [astro-ph/0512089].
- [20] S. Jung and C. S. Shin, “Gravitational-Wave Lensing Fringes by Compact Dark Matter at LIGO,” arXiv:1712.01396 [astro-ph.CO].
- [21] T. T. Nakamura, “Gravitational lensing of gravitational waves from inspiraling binaries by a point mass lens,” *Phys. Rev. Lett.* **80**, 1138 (1998). doi:10.1103/PhysRevLett.80.1138
- [22] P. W. Graham and S. Jung, “Localizing Gravitational Wave Sources with Single-Baseline Atom Interferometers,” *Phys. Rev. D* **97**, no. 2, 024052 (2018) doi:10.1103/PhysRevD.97.024052 [arXiv:1710.03269 [gr-qc]].
- [23] R. Nair and T. Tanaka, “Synergy between ground and space based gravitational wave detectors. Part II: Localisation,” *JCAP* **1808**, no. 08, 033 (2018) doi:10.1088/1475-7516/2018/08/033 [arXiv:1805.08070 [gr-qc]].
- [24] S. Isoyama, H. Nakano and T. Nakamura, “Multiband Gravitational-Wave Astronomy: Observing binary inspirals with a decihertz detector, B-DECIGO,” *PTEP* **2018**, no. 7, 073E01 (2018) doi:10.1093/ptep/pty078 [arXiv:1802.06977 [gr-qc]].
- [25] R. Takahashi and T. Nakamura, “Deci hertz laser interferometer can determine the position of the coalescing binary neutron stars within an arc minute a week before the final merging event to black hole,” *Astrophys. J.* **596**, L231 (2003) doi:10.1086/379112 [astro-ph/0307390].
- [26] H. G. Choi and S. Jung, “A New Probe of Dark Matter-Induced Fifth Force with Neutron Star Inspirals,” arXiv:1810.01421 [hep-ph].
- [27] Schneider, P., Ehlers, J., & Falco, E. E., “Gravitational Lenses,” Springer-Verlag Berlin Heidelberg New York (1992)
- [28] T. Nakamura and S. Deguchi “Wave Optics in Gravitational Lensing,” *Prog. Theor. Phys. Suppl.* **133**, 137 (1999)
- [29] I. Ferrndez-Nez and O. Bulashenko, “Emergence of Fresnel diffraction zones in gravitational lensing by a cosmic string,” *Phys. Lett. A* **381**, 1764 (2017) doi:10.1016/j.physleta.2017.03.046 [arXiv:1612.07218 [astro-ph.CO]].
- [30] J. B. Keller, “Gravitational lensing by cosmic string loops,” *J. Opt. Soc. Am.* **52**, 2 (1962)
- [31] R. R. Caldwell and B. Allen, “Cosmological constraints on cosmic string gravitational radiation,” *Phys. Rev. D* **45**, 3447 (1992). doi:10.1103/PhysRevD.45.3447
- [32] K. J. Mack, D. H. Wesley and L. J. King, “Observing cosmic string loops with gravitational lensing surveys,” *Phys. Rev. D* **76**, 123515 (2007) doi:10.1103/PhysRevD.76.123515 [astro-ph/0702648 [ASTRO-PH]].
- [33] J. J. Blanco-Pillado, K. D. Olum and B. Shlaer, “The number of cosmic string loops,” *Phys. Rev. D* **89**, no. 2, 023512 (2014) doi:10.1103/PhysRevD.89.023512 [arXiv:1309.6637 [astro-ph.CO]].
- [34] A. Vilenkin, “Cosmic strings as gravitational lenses,” *Astrophys. J.* **282**, L51 (1984). doi:10.1086/184303
- [35] P. Christian, S. Vitale and A. Loeb, “Detecting Stellar Lensing of Gravitational Waves with Ground-Based Observatories,” arXiv:1802.02586 [astro-ph.HE].
- [36] L. Dai, S. S. Li, B. Zackay, S. Mao and Y. Lu, “Detecting Lensing-Induced Diffraction in Astrophysical Gravitational Waves,” arXiv:1810.00003 [gr-qc].
- [37] K. Belczynski, D. E. Holz, T. Bulik and R. O’Shaughnessy, “The first gravitational-wave source from the isolated evolution of two 40-100 Msun stars,” *Nature* **534**, 512 (2016) doi:10.1038/nature18322 [arXiv:1602.04531 [astro-ph.HE]].
- [38] <http://www.syntheticuniverse.org/stvsgwo.html>
- [39] B. P. Abbott *et al.* [LIGO Scientific and Virgo Collaborations], “GW150914: The Advanced LIGO Detectors in the Era of First Discoveries,” *Phys. Rev. Lett.* **116**, no. 13, 131103 (2016) doi:10.1103/PhysRevLett.116.131103 [arXiv:1602.03838 [gr-qc]].

- [40] S. Hild *et al.*, “Sensitivity Studies for Third-Generation Gravitational Wave Observatories,” *Class. Quant. Grav.* **28**, 094013 (2011) doi:10.1088/0264-9381/28/9/094013 [arXiv:1012.0908 [gr-qc]].
- [41] P. W. Graham, J. M. Hogan, M. A. Kasevich and S. Rajendran, “Resonant mode for gravitational wave detectors based on atom interferometry,” *Phys. Rev. D* **94**, no. 10, 104022 (2016) doi:10.1103/PhysRevD.94.104022 [arXiv:1606.01860 [physics.atom-ph]].
- [42] P. W. Graham *et al.* [MAGIS Collaboration], “Mid-band gravitational wave detection with precision atomic sensors,” arXiv:1711.02225 [astro-ph.IM].
- [43] K. Yagi and N. Seto, “Detector configuration of DECIGO/BBO and identification of cosmological neutron-star binaries,” *Phys. Rev. D* **83**, 044011 (2011) Erratum: [*Phys. Rev. D* **95**, no. 10, 109901 (2017)] doi:10.1103/PhysRevD.95.109901, 10.1103/PhysRevD.83.044011 [arXiv:1101.3940 [astro-ph.CO]].
- [44] R. Takahashi and T. Nakamura, “Wave effects in gravitational lensing of gravitational waves from chirping binaries,” *Astrophys. J.* **595**, 1039 (2003) doi:10.1086/377430 [astro-ph/0305055].
- [45] A. Gould, “Femtolensing of gamma-ray bursters,” *Astrophys. J.* **386**, L5 (1992) doi:10.1086/186279
- [46] A. Barnacka, J. F. Glicenstein and R. Moderski, “New constraints on primordial black holes abundance from femtolensing of gamma-ray bursts,” *Phys. Rev. D* **86**, 043001 (2012) doi:10.1103/PhysRevD.86.043001 [arXiv:1204.2056 [astro-ph.CO]].
- [47] N. Matsunaga and K. Yamamoto, “The finite source size effect and the wave optics in gravitational lensing,” *JCAP* **0601**, 023 (2006) doi:10.1088/1475-7516/2006/01/023 [astro-ph/0601701].
- [48] O. S. Sazhina, M. V. Sazhin, V. N. Sementsov, “Cosmic microwave background anisotropy induced by a moving straight cosmic string,” *J. Exp. Theor. Phys.* **106**, 878 (2008) doi:10.1134/S1063776108050051
- [49] B. Shlaer and S.-H. H. Tye, “Cosmic string lensing and closed time-like curves,” *Phys. Rev. D* **72**, 043532 (2005) doi:10.1103/PhysRevD.72.043532 [hep-th/0502242].
- [50] B. P. Abbott *et al.* [LIGO Scientific and Virgo Collaborations], “Tests of general relativity with GW150914,” *Phys. Rev. Lett.* **116**, no. 22, 221101 (2016) Erratum: [*Phys. Rev. Lett.* **121**, no. 12, 129902 (2018)] doi:10.1103/PhysRevLett.116.221101, 10.1103/PhysRevLett.121.129902 [arXiv:1602.03841 [gr-qc]].